ACS OMEGA

Open Access

http://pubs.acs.org/journal/acsodf

Article

Intercalation vs Adsorption Strategies of Myo-Inositol Hexakisphosphate into Zn−Fe Layered Double Hydroxide: A Tiff between Anion Exchange and Coprecipitation

Rimjim Gogoi, Madhusmita Baruah, Arup Borgohain, Jiban Saikia,* Vishwa Jyoti Baruah, Satter Rohman, Mohini Singh, Rahul Kar, Sandeep Kumar Dey, Bhaskar Mazumder, and Tanmoy Karak*

Cite This: *ACS Omega* 2023, 8, 43151−43162

Read Online

ACCESS | Metrics & More | Article Recommendations | Supporting Information

ABSTRACT: Myo-inositol hexakisphosphates (IHPs) or phytates are the most abundant organic phosphates having the potential to serve as a phosphorus reserve in soil. Understanding the fate of IHP interaction with soil minerals tends to be crucial for its efficient storage and utilization as a slow-release organic phosphate fertilizer. We have systematically compared the effective intercalation strategy of a phytate onto Zn−Fe layered double hydroxide (LDH) acting as storage/carrier material through coprecipitation and anion exchange. Powder X-ray diffraction, X-ray photoelectron spectroscopy, elemental analysis, thermogravimetric analysis, FTIR spectra, and molecular modeling demonstrated the formation of phytate-intercalated Zn−Fe LDH through coprecipitation with a maximum loading of 41.34% (w/w) in the pH range of ∼9−10 in a vertical alignment through monolayer formation. No intercalation product was obtained from the anion exchange method, which was concluded based on the absence of shifting in the XRD (003) peak. A change in the zeta potential values from positive to negative and subsequent increase in solution pH, with decreasing phytate concentration, are suggestive of adsorption of IHP onto the LDH surface. The batch adsorption data were best fitted with Langmuir isotherm equation and followed the pseudo-second-order kinetic model. The maximum adsorption capacity was found to be 45.87 mg g^{-1} at a temperature of 25 ± 0.5 °C and pH 5.63.

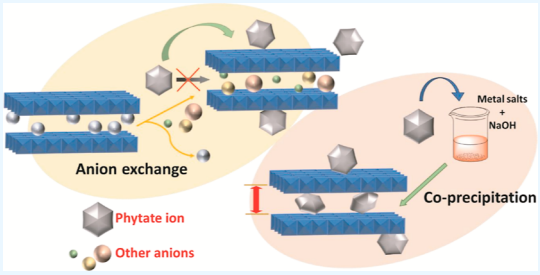

1. INTRODUCTION

In the last few decades, the application of inorganic phosphorus (P) fertilizers has witnessed an exponential increase owing to its exceeding demand. Limited mineral reserves and permanent P losses from leaching, runoff, soil erosion, and fixation reactions have triggered great concern.[1−4] Emphasis on the exploration of an abundant and sustainable source of P for fertilizer applications are imperative. Organic phosphates (OPs) account for ∼20−80% of the total phosphorus content in the form of nucleic acids, phospholipids, sugar phosphates, and inositol phosphates in most soils and sediments, which could be a good choice of inorganic P substitutes.[3,5]

Among all other forms, inositol phosphates make up half of the organic phosphate.[6] Myo-inositol hexakisphosphate (IHP) or phytate (Figure 1), a 6-fold dihydrogen phosphate monoester of inositol (a 6-fold alcohol of cyclohexane)[7] is the most abundant inositol phosphate[8,9] in nature. It carries a high negative charge owing to the presence of six phosphate groups attached to the six carbon atoms of the inositol ring. The presence of the six phosphate groups primarily contributes to the strong chelating ability of IHP toward divalent and trivalent metal ions, oxides, and clay surfaces in soil.[2,8] The structure of IHP is shown in Figure 1 presenting Mills projection for IHP (1a), three-dimensional 1-axial−5-equatorial conformation for IHP[7] (1b), and the optimized structure of IHP in these two respective forms (1c and 1d). A number of studies have reported the interaction of IHP with active soil minerals including metal hydroxides ($Al(OH)_3$),[8,10] metal oxides (goethite),[11] hematite,[12] and kaolinite[13,14] through adsorption/desorption and surface precipitation. Preferential accumulation of IHP in soil due to complexation with metal ions and clay surfaces obstructs its biodegradation,[5,6] causing P scarcity and rendering all the participating elements unavailable for plant uptake. Thus, it holds remarkable potency in understanding the interaction of IHP with potential storage and carrier materials and its efficient loading and release for utilization in phosphorus delivery.

Layered double hydroxides (LDHs) are a class of synthetic clay materials analogous to naturally occurring hydrotalcite-like clay minerals.[15−18] They are structured with sheets of dipositive and tripositive ions having charge-compensating

Received: September 7, 2023
Revised: October 1, 2023
Accepted: October 23, 2023
Published: November 3, 2023

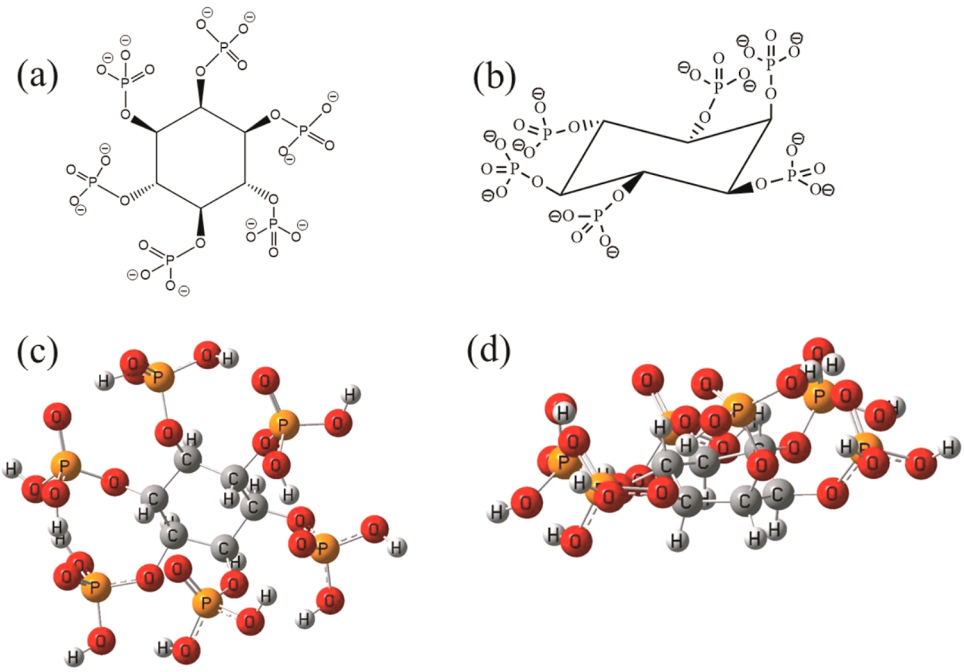

Figure 1. Structure of IHP: Mills projection (a), three-dimensional 1-axial−5-equatorial conformation (b), and optimized structures in respective forms (c,d).

anions residing in between the sheets along with hydroxide ions and water molecules.[19,20] They have an excellent ability to incorporate a broad range of organic and inorganic anions through intercalation into their basal layers. With their large aspect ratio, LDH materials have proven to be very efficient agents in storage and protection of the intercalated moiety in their gallery region owing to their layered sheet structure and subsequent slow delivery.[21] Because of their nontoxic nature, the LDHs are reported to have acted as slow-release agents in agriculture[21−24] and drug delivery.[25−27] Not much work has been reported showcasing the interaction of LDH components with the IHP moiety for agricultural utilization. Wang et al.[4] investigated the retention of IHP in soil to reduce P loss risk in the presence of Mg−Al LDH. They witnessed the adsorption of IHP on the LDH surface but no intercalation into the basal layers. However, a number of studies have demonstrated synthesis of IHP-intercalated LDH materials by different routes for application in metal ion capture,[28] corrosion inhibition,[29] and flame retardancy.[30] An understanding of the nature of interaction of IHP with LDH materials and detailed study on the formation of a probable intercalation product of IHP in LDH basal structures may provide a way for advanced future application of these cost-effective and biofriendly materials in retention and delivery of phytate ions as agricultural products.

The present work demonstrates a systematic study for intercalation of IHP into Zn−Fe LDH structure through coprecipitation and anion exchange methods. IHP-intercalated LDH has the potential to act as a sustainable P storage and delivery vehicle. The choice of cations for LDH synthesis was done because eventual dissolution of LDH does not dispense any harmful elements into the environment, and the elements could be utilized by plants. Characterization techniques including powder X-ray diffraction (PXRD), Fourier transform infrared (FTIR) analysis, thermogravimetric analysis (TGA), inductively coupled plasma− mass spectrometry (ICP−MS), scanning electron microscopy− energy-dispersive x-ray analysis (SEM−EDX), high-resolution transmission electron microscopy (HRTEM), and X-ray photoelectron spectroscopy (XPS) were used for investigation of the structure of the obtained products. A batch study for the adsorption of IHP on the synthesized Zn−Fe−Cl LDH surface was carried out to gain insight into the interaction of IHP with the LDH surface. A measurement of zeta potential, solution pH, and spectrophotometric assay was performed to gain understanding about its underlying mechanism. To probe the minimum energy structure of phytic acid for investigation of the intercalation process, geometry optimization calculation of the molecule was carried out using density functional theory (DFT).

2. METHODOLOGY

2.1. Materials. AR-grade chemicals including $ZnCl_2{\cdot}6H_2O$ (CAS: 7646-85-7), $FeCl_3{\cdot}6H_2O$ (CAS: 10025-77-1), NaOH (CAS: 1310-73-2), and NaCl (CAS: 7647-14-5) were purchased from FINAR, Gujarat, India. Sodium phytate (CAS: 17211-15-3, molecular weight: 923.81 g mol^{-1}) was purchased from SRL, Maharashtra, India. The water has been purified by a Millipore water purification system (MΩ cm^{-1} conductivity, 18.2 Milli-Q Lab Water Solutions) and was used for all the solution preparation and syntheses.

2.2. Synthesis of Parent Zn−Fe-LDH (ZLDH). Zn−Fe−Cl LDH (ZLDH) nanomaterial was synthesized by coprecipitation,[31,32] under a N_2 atmosphere and at 70 °C reaction temperature, followed by ultrasonication method with an aging time of 17 h with a Zn/Fe molar ratio of 3:1. The product was separated by centrifugation, washed repeatedly with ultrapure water, and dried in a vacuum desiccator.

2.3. Intercalation through Coprecipitation. To inspect the probable intercalation of IHP in the lamellar region of LDH, the precursor solution in ultrapure water containing $ZnCl_2$ and $FeCl_3$ in the ratio 3:1 was added to sodium phytate solution (IHP source), with variable reaction parameters

https://doi.org/10.1021/acsomega.3c06788
ACS Omega 2023, 8, 43151−43162

during the precipitation of the double hydroxides under a N_2 atmosphere, with dropwise addition of 2 M NaOH solution. The reaction temperature was set at 70 °C. The product formed was aged in the mother liquid for 24 h. The products (Table 1) were collected by centrifugation, followed by repeated washing with ultrapure water, and then dried in a vacuum desiccator. The final pH of each system was monitored. The reaction volume in Table 1 refers to the total volume of mixed metal solution and sodium phytate solution, excluding the volume of NaOH.

Table 1. Products Obtained during the Precipitation of IHP with LDH Precursors

products obtained	Zn^{2+}/Fe^{3+}/IHP ratio	reaction volume (mL)	IHP quantity (M)	aging time (h)	final pH
Z1	3:1:1	120	0.025	24	∼9−10
Z2	3:1:0.4	120	0.01	24	∼10−11
Z3	3:1:0.4	60	0.01	24	∼8−10
Z4	3:1:0.4	60	0.025	24	∼7−8
Z5	3:1:0.4	60	0.03	24	∼7−8

The basal spacing (d) and interlayer spacing or the gallery height (L) for the characteristic (003) plane of the products from PXRD patterns were calculated.

The basal spacing (d) was calculated from Bragg's equation.

$$d = \frac{\lambda}{2\sin\theta} \tag{1}$$

The gallery height (L) was calculated from basal spacing value by subtracting the value of LDH layer thickness taken to be 0.48 nm for hydrotalcite-like materials.[33,34]

$$\text{Gallery height } (L) = \text{basal spacing } (d) - \text{layer thickness} \tag{2}$$

2.4. Intercalation through Anion Exchange. The possible intercalation of IHP in the basal layers of synthesized Zn−Fe LDH (ZLDH) was studied through anion exchange with the interlayer Cl^- ions of the LDH. Weighed quantities of ZLDH were added to sodium phytate solution with varying concentrations under a nitrogen atmosphere. The products obtained were centrifuged and washed repeatedly with ultrapure water. The supernatant was used for spectrophotometric determination of IHP remained in solution. The products (Table 2) were dried in a vacuum desiccator and stored for further analyses.

2.5. Sorption Experiments. To probe the nature and underlying mechanism for the interaction of IHP with synthesized ZLDH, sorption experiments were carried out.

2.5.1. Preparation of IHP Stock Solution. A stock solution (5 mM) of sodium phytate was prepared in ultrapure water and diluted to get the desired concentration. Calibration curves for phytate were obtained by measuring the absorbance at 500 nm. Hydrochloric acid (HCl) and sodium hydroxide (NaOH) solutions were used to adjust the pH in the desired range of investigation.

Table 2. Products Obtained after the Exchange Experiment of IHP with ZLDH

products obtained	temperature (°C)	ZLDH amount (mg)	IHP quantity (M)	exchange time
ZAP1	75	300	0.01	5 min
ZAP2	75	300	0.01	30 min
ZAP3	75	300	0.05	24 h
ZAP4	75	300	0.1	6 h
ZAP5	75	300	0.1	24 h

Sorption studies were done using batch experiment methods. The ZLDH sample (200 mg) was weighed and suspended in half the solvent (ultrapure water) of the total fixed volume of the IHP solution (30 mL). The suspension was ultrasonicated for homogenization, and then, the other half of the adsorbate solution was added to it with required IHP concentration. The resultant solution was shaken for 24 h to achieve equilibrium at a temperature of 25 ± 0.5 °C. The experiment was conducted with different initial adsorbate concentrations for isotherm studies and at different reaction times for kinetics studies. After each experiment, half of the aliquot was withdrawn, centrifuged, and filtered through a 0.22 μm membrane filter and used for spectrophotometric determination of IHP as described by Agostinho et al.[35] The other half was used for the investigation of the zeta potential values. The pH changes after sorption at different time intervals were investigated to evaluate the nature of the interaction taking place. Post experimental ZLDH samples were dried in a vacuum desiccator and stored for further analyses. The effect of pH on the sorption nature was studied with constant IHP concentration in the LDH suspension, followed by observation of changes in the zeta potential values. The amount of IHP sorbed was calculated by the difference in phytate concentration measured before and after adsorption equilibrium was reached.

The amount of IHP sorbed at equilibrium was calculated from eq 3.

$$Q_e = \frac{(C_0 - C_t)V}{m} \tag{3}$$

where Q_e is the maximum sorption capacity (mg g^{-1}); C_0 (mg L^{-1}) and C_t (mg L^{-1}) are the initial and equilibrium IHP concentration, respectively; V is the volume of the solution (L); and m is the weight of the sorbent (g).[36,37]

The sorption isotherms were fitted with the Langmuir and Freundlich model. The linear forms of the Langmuir model, the Langmuir Linearization 1 plot of Hanes−Woolf plot (eq 4), and the Freundlich model (eq 5) are represented with the following equations.

$$\frac{C_e}{Q_e} = \frac{1}{K_L Q_m} + \frac{C_e}{Q_m} \tag{4}$$

$$\ln\ Q_e = \ln\ K_F + \frac{1}{n}\ln\ C_e \tag{5}$$

where Q_m (mg g^{-1}) and K_L (L mg^{-1}) are constants corresponding to adsorption capacity and net enthalpy of adsorption, respectively, and K_f and n are the constants representing the adsorption capacity and intensity of adsorption, respectively.[38]

Lagergren pseudo-first-order (eq 6) and pseudo-second-order (eq 7) kinetic models were fitted to simulate the sorption kinetics data.

$$\ln(q_e - q_t) = \ln\ q_e - k_1 t \tag{6}$$

https://doi.org/10.1021/acsomega.3c06788
ACS Omega 2023, 8, 43151−43162

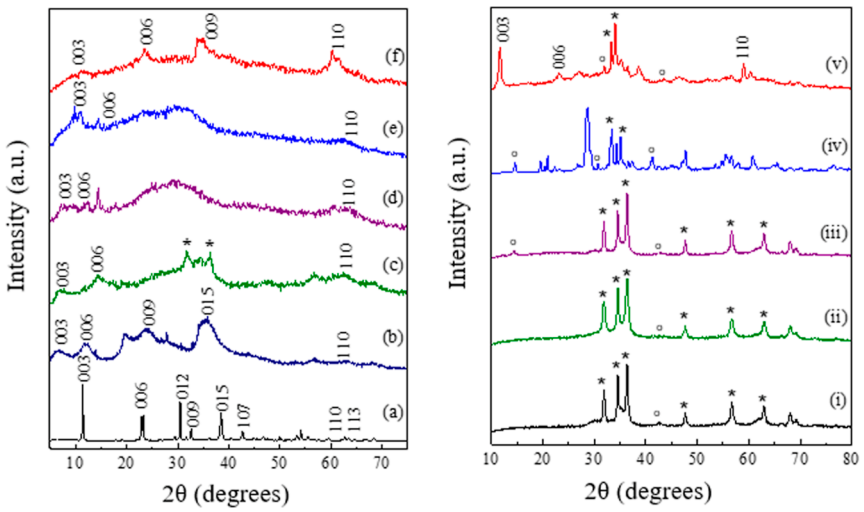

Figure 2. PXRD patterns for (a) ZLDH, (b) Z1, (c) Z2, (d) Z3, (e) Z4, and (f) Z5; (i) A1, (ii) A2, (iii) A3, (iv) A4, and (v) A5 [* = ZnO and ° = $ZnFe_2O_4$].

$$\frac{t}{q_t} = \frac{t}{q_e} + \frac{1}{k_2 q_e^2} \quad (7)$$

where q_e (mg g^{-1}) and q_t (mg g^{-1}) are the amount of IHP sorbed per unit mass of ZLDH at equilibrium and time t, respectively; K_1 (min^{-1}) is the pseudo-first-order rate constant; and K_2 (g mg^{-1} min^{-1}) is the second-order constant for sorption.[39]

2.6. Characterization. The FTIR spectra of the samples were recorded in an FTIR spectrometer (Agilent Model no: Cary 630, USA; SL. no. MY20192018) in the range of 400−4000 cm^{-1}. The TGA thermograms of the samples were obtained using a thermogravimetric analyzer (Hitachi STA7300, USA) in the temperature range of 25−700 °C at a heating rate of 10° per minute under a N_2 atmosphere. The PXRD analyses of the samples were performed in an X-ray diffractometer (Bruker Model D8 Advance A25, Germany) using monochromatic Cu Kα radiation (λ = 1.54056 Å). The X-ray photoelectron spectra were recorded using ESCALAB Xi + model (Thermo Fisher Scientific, Pvt. Ltd., UK). The HRTEM micrograph of samples was recorded using an electron microscope (JEOL-JEM 2100, Japan) with an accelerating voltage of 200 kV. The SEM−EDX analysis was performed using a JEOL JSM-IT300 Scanning Electron Microscope. ICP−MS analysis was performed for quantification of the P content in phytate-loaded samples using ICP-Mass spectrometer (Agilent 7900, US). The ζ potential variations of the investigated samples were measured using the Anton Paar Particle Analyzer Litesizer 500 (Anton Paar, US). For all the analytical purposes, spectrophotometric methods were employed using a Multiskan SkyHigh Microplate Spectrophotometer (A51119700DPC, Thermo Fisher Scientific, Pvt. Ltd., UK) in the range of 300−800 nm.

2.7. DFT Calculations. The structure of myo-inositol hexakisphosphate in the form of phytic acid was optimized in the ground state using the B3LYP functional and 6-31G(d) basis set (Table S1). The choice of phytic acid instead of phytate anion was made for simplicity of optimization. Along with geometry optimization, vibrational frequency calculations have been performed to characterize the nature of stationary point, and no imaginary frequencies have been observed. The minimum energy structure was obtained without applying any symmetry restrictions. All calculations were performed using Gaussian 09 software package.[40] The distances between oxygen atoms from the optimized structure were calculated and are given in Table S2.

3. RESULTS AND DISCUSSION

3.1. Characterization of Parent Zn−Fe LDH. The parent Zn−Fe LDH (ZLDH) was characterized prior to other intercalates for reference. The XRD spectra for ZLDH confirm the presence of layered structure formation with well-defined sharp and intense peaks characteristic of LDH materials at lower 2θ value and less intense peaks at higher 2θ values[41] (Figure 2a). Peaks observed at the (003), (006), (012), (009), (015), (110), and (113) planes establish the formation of highly -crystalline LDH structure (JCPDS-00-048-1026).[42] The basal spacing (d_{003}) is calculated to be 0.778 nm, a value typical of Cl^--intercalated LDH.[43,44] The ratio of Zn/Fe from the EDX spectra is observed as 2.57 (Figure S1a and Table S3). The XPS survey spectrum shows (Figure S2a) the presence of all required elements. Characteristic peak (Figure S3) at binding energy (eV) values of 1021.5 and 1044.8 for $2p_{3/2}$ and $2p_{1/2}$ states, respectively, shows the presence of Zn^{2+}.[45,46] Peaks at 710.718 and 723.68 eV with satellite peaks at 717.65 and 732.84 eV confirm the presence of Fe^{3+}.[47] The SEM micrograph for ZLDH shows the formation of a multilayer stacked structure with intensely agglomerated particles (Figure 3a). The formation of nanosized particles (with an average diameter of ∼20 nm) with an aggregated nature is established by the HRTEM images (Figure 3b).

3.2. Coprecipitation Behavior of IHP in Zn−Fe Precipitates. Coprecipitation is a one-pot method for the synthesis of LDHs, with simultaneous precipitation of $M(OH)_2$ and $M(OH)_3$ by addition of a precipitating reagent. It is convenient for large-scale LDH production and for intercalation of a variety of anionic groups in the LDH lamellar structure, especially complex organic moieties.

The formation of intercalated products was investigated with the PXRD technique to observe the changes in crystal pattern of the LDH structures. The shifting of the (003) reflection in the X-ray diffractogram, responsible for change in basal spacing (calculated from eq 1, given in Table 3), was primarily monitored for the observation of intercalation of IHP in the

https://doi.org/10.1021/acsomega.3c06788
ACS Omega 2023, 8, 43151−43162

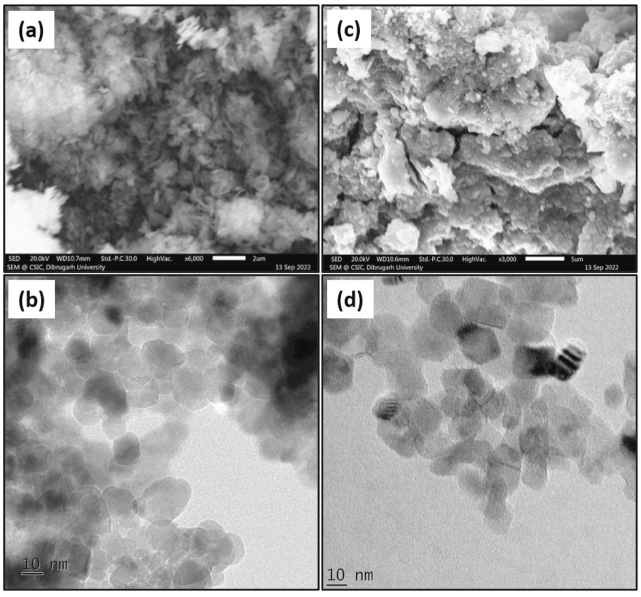

Figure 3. SEM (a,c) and HRTEM (b,d) micrographs for ZLDH and Z1, respectively.

Table 3. Values of Crystal Parameters for the Intercalated Samples

samples	d_{003} (c_0) (nm)	interlayer spacing (L) (nm)	"c" parameter (nm)	d_{110} (a_0) (nm)	"a" parameter (nm)
ZLDH	0.778	0.298	2.334	0.155	0.310
Z1	1.375	0.895	4.125	0.150	0.300
Z2	1.242	0.762	3.726	0.151	0.302
Z3	1.184	0.704	3.552	0.151	0.302
Z4	0.895	0.415	2.64	0.150	0.300
Z5	0.880	0.400	2.685	0.152	0.304

LDH layers. The basal spacing is correlated to the thickness of a single metal hydroxide layer, which depends upon the size and orientation of the intercalated species. In Figure 2, the shifting of (003) and (006) planes to lower 2θ value is observed for Z1-Z5. The product Z1 exhibits the highest shift for the (003) plane from 11.4° in ZLDH to 6.44° 2θ angles giving a basal spacing (d_{003}) of 1.375 nm. This infers to an expansion of the LDH sheets with increased interlayer spacing owing to the successful insertion of an IHP moiety into the lamellar region. The final pH of the Z1 medium was measured to be ~9−10. In the case of Z2 and Z3, a d_{003} shift of 1.24 and 1.184 nm were observed, respectively. Small d-spacing shifts were observed for Z4 and Z5 samples, and the values resemble the d-spacing values for phosphate-intercalated LDHs.[4] The interlayer spacing calculated from eq 2 is highest for Z1 sample followed by Z2 > Z3> Z4> Z5 (Table 3). The basal repeat distance "c" and supercell parameter "a" are calculated as $c = 3d_{003}$ and $a = 2d_{110}$[48] for the samples and are listed in Table 3. A broadening of peak corresponding to the (01l) plane around mid-two theta angles refers to stacking faults occurring due to the simultaneous formation of LDH and rearrangement of the bulky phytate anion.[49] The merging of the (110) and (113) planes in the diffractograms of the intercalated structures also signifies a disorganization of the layered structure.[50] Other literature also suggest the shifting of the (003) plane toward lower 2θ angles with broadening of the XRD peaks and disruption in layered structures upon insertion of organics.[51] Moreover, the increase in gallery height and emergence of halo and amorphous peak refer to partial delamination of the LDH structure.

The appearance of an additional peak assigned to the ZnO phase in the diffractogram of the Z2 sample may be ascribed to an increase in solution pH (~11). The formation of ZnO phase arises during coprecipitation at pH exceeding 10.[52] However, the products with lesser final pH values exhibit reduced d-shifting values, indicating incomplete and lower extent of intercalation (Z4−Z5). The solution pH was governed by the rate and duration of addition of metal salt solution and NaOH, in addition to the initial IHP concentration and quantity of the reaction volume. Lower reaction volume was observed to exhibit greater pH fluctuations. Coprecipitation at pH greater than 11 led to the loss of LDH structure and formation of oxide phases [Figure 2i−iv]. At pH ~11−13, mixed metal oxide phase is observed without the formation of hydrotalcite phase [Figure 2iii,iv]. On further increasing the pH, formation of only ZnO phase is observed [Figure 2i,ii]. This occurs due to the preferential formation of ZnO and dissolution of $Zn(OH)_2$ at high pH conditions.[53] Coprecipitation in the presence of abundant $Na_2(CO_3)_2$ solution in similar reaction conditions as Z1 did not result in IHP-intercalated product, as carbonate ions compete for the basal layers, which have higher affinity compared to IHP (Figure 2v). Furthermore, addition of $Na_2(CO_3)_2$ leads to an increase in the solution pH, which subsequently resulted in the appearance of a mixed oxide phase in the diffractogram.

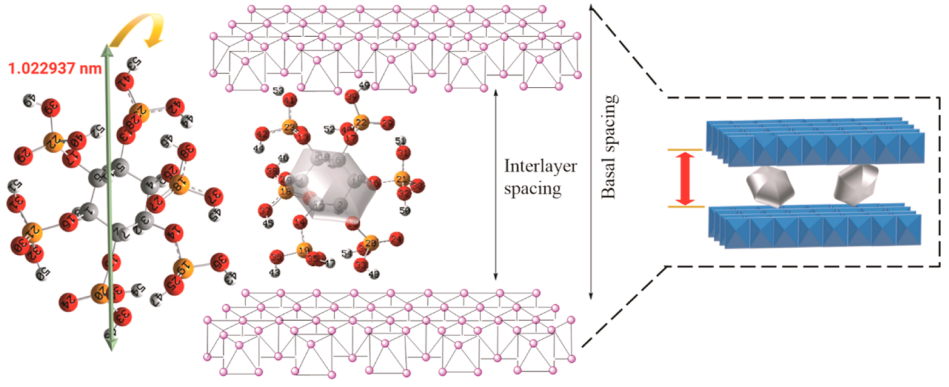

Figure 4. Proposed orientation of the IHP inside the LDH interlayer spacing.

https://doi.org/10.1021/acsomega.3c06788
ACS Omega 2023, 8, 43151−43162

The obtained basal spacing value (1.375 nm) for Z1 coincides well with the reported phytate-intercalated LDH.[29] The interlayer spacing from eq 2 is calculated to be 0.895 nm, lesser than the highest O−O bond distance (from C2−C5) found as 1.022937 nm from the optimized phytic acid structure. This indicates that IHP is intercalated in a vertical monolayer formation in the LDH interlayers, cross-linking the LDH sheets through electrostatic bonding with the phosphate groups (Figure 4) but in a tilted way to accommodate itself. As shown in Table S2, IHP may orient in C1−C3, C2−C5, or C3−C6 opposite endings, giving an O−O distance higher than the gallery height of Z1.

The XPS survey spectrum for Z1 exhibits P 2p peak at a binding energy value of 132.21 eV, implying successful loading of IHP into LDH (Figure S2b). From ICP−MS analysis, the percentage loading of IHP was calculated to be 41.34% (w/w). The O 1s XPS spectra for Z1 (Figure S5b) deconvoluted to three peaks at binding energy values of 528.84, 530.13, and 531.64 eV, respectively, assigned to lattice O_2, surface −OH, and nonbridging oxygen (P−O, Zn−O), which further confirms the insertion of the IHP moiety.[42] The appearance of a peak for Cl in the survey spectrum indicates that some quantity of Cl^- ions was inherently intercalated in the interlayers along with IHP. The absence of a Na peak in the survey spectrum of Z1 refers to the absence of pure phase phytate salt, indicating complete insertion.

The SEM image for Z1 (Figure 3c) shows the formation of a less aggregated deformed sheet-like morphology, whereas formation of a less agglomerated nanostructure was shown by the HRTEM micrograph (Figure 3d), indicating insertion of IHP inside the LDH layers.

The formation of intercalated product Z1 is further supported by the FTIR spectra (Figure 5). Peaks typical of

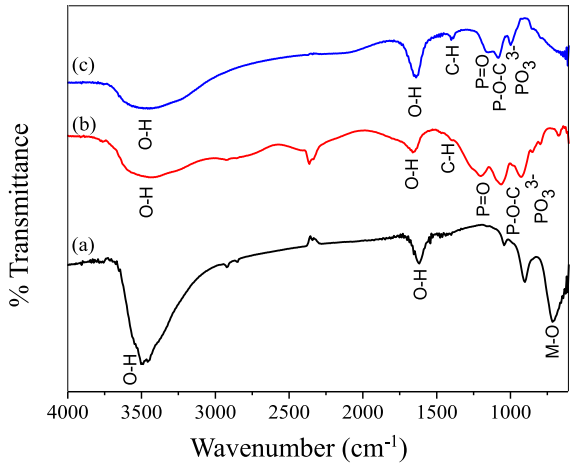

Figure 5. FTIR spectra for (a) ZLDH, (b) sodium phytate, and (c) Z1.

layered structure appeared at ∼3400 cm^{-1} due to stretching vibration of metal hydroxides and trapped H_2O molecules, at ∼1643 cm^{-1} due to bending vibration of the interlayer H_2O molecules and around 500−800 cm^{-1} due to the M−O stretching vibration for Z1 in reference to ZLDH. Characteristic peaks owing to P═O, P−O−C, and PO_3^{3-} stretching modes are observed around 1152, 1087, and 1000, respectively, for Z1 implies the binding of the phytate moiety;[28] signifying intercalation of IHP in the interlayer of the LDH. The FTIR spectra for Z2−Z5 are given in Figure S7.

The TGA and derivative thermogravimetry (DTG) thermograms in Figure 6 demonstrate the comparative weight loss profiles of Z1, Z2, and A4 with ZLDH as the reference. It can be observed that both Z1 and Z2 exhibit two distinct breaks, similar to ZLDH, at temperature ranges 100−250 and 250−700 °C. In case of ZLDH, the first weight loss stage is observed because of desorption of the physically adsorbed water, whereas the second weight loss occurs due to the dehydroxylation of the LDH layers and decomposition of the interlayer anions, a pattern typical of LDH structures.[29] The first break observed for Z1 can be ascribed to the evaporation of water, and the second break denotes the disruption of the hydroxide layers and intercalated IHP anion. The IHP-intercalated sample Z1 retained larger weight (77.185%) compared to that in ZLDH (61.2%), probably owing to the formation of a thermally stable cross-linking network by IHP with LDH layers at higher temperatures.[30] The weight loss profile for Z2 can be described similar to that of Z1, but Z2 retained less weight (65.94%) partially due to the existence of mixed phase structures. The thermogram for sample A4 shows typical weight loss profile for mixed metal oxides, exhibiting one distinct break owing to the evaporation of the water molecules on the exterior of the metal oxide structures.[54] This further confirms the formation of a mixed oxide phase rather than an LDH phase, as indicated by the PXRD patterns (Figure 2iv).

3.3. Interaction through Anion Exchange. Intercalation of IHP in the LDH lamellar region through ion exchange with precursor Cl^- ions was investigated with varying parameters (Table 2). The intercalation process was inspected by monitoring the shift in the characteristic (003) reflection in the X-ray diffractogram of the exchange products. The sharp and symmetric reflections in the PXRD patterns for ZLDH (Figure 2a) are lost after exchange experiments with the IHP moiety. The XRD patterns (Figure 7) exhibit a broad, halo, and amorphous peak in the (01*l*) 2θ region. It can be inferred to the probable dissolution of the LDH component in the solid−liquid interface[55] and possible binding with the highly charged phytate ion. However, the absence of the (003) peak shifting to lower 2θ angles signifies no expansion in the LDH interlayer spacing by insertion of the IHP moiety replacing the existing Cl^- ions. This accordingly suggests that the formation of IHP-intercalated Zn−Fe LDH through ion exchange could not be achieved. Nevertheless, likely interaction of ZLDH with phytate ions without intercalation may be incurred as observed from the PXRD patterns.

As the IHP moiety is expected to interact through its phosphate groups with the LDH component, the peaks corresponding to P−O bond stretching are monitored in the FTIR spectra of the exchange products. The appearance of new peaks assigned to P═O, P−O−C, and M−O are observed as shown in Figure 8, further suggesting the interaction of IHP with LDH. The bands correlated to the P═O and P−O−C vibrational modes experienced a shift from the original wavenumber in its sodium phytate structure (Figure 5). This can be ascribed to the formation of the inner-sphere complex at the LDH surface as phosphate groups are cited to bind to metal ions at hydroxide surface through inner-sphere complex formation.[2]

The XPS survey spectrum for ZAP1 and ZAP5 further confirms the presence of P in the LDH surface (Figure S2c,d).

https://doi.org/10.1021/acsomega.3c06788
ACS Omega 2023, 8, 43151−43162

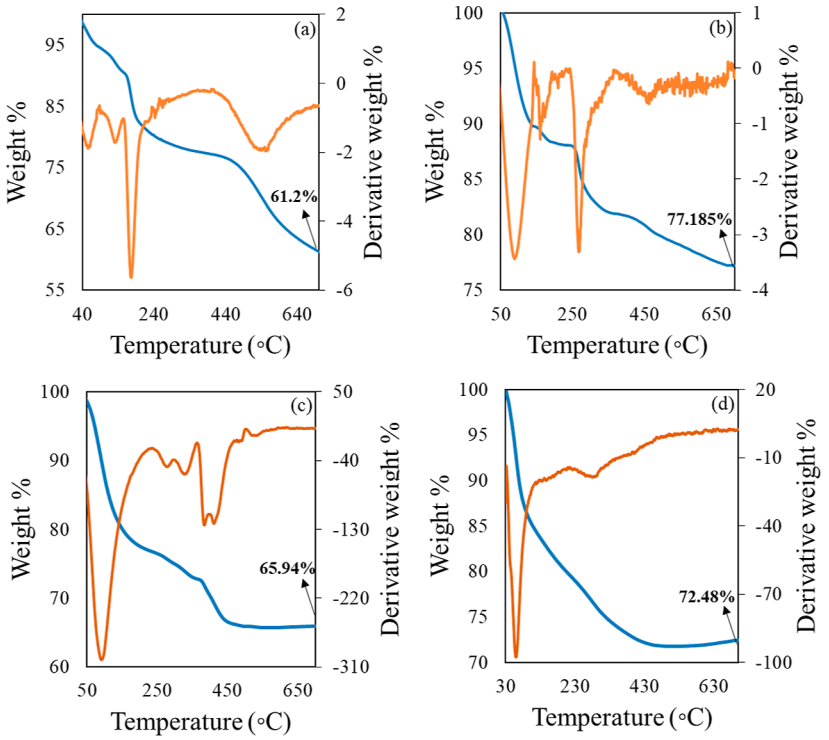

Figure 6. TGA and DTG thermogram for (a) ZLDH and (b) Z1, (c) Z2 and (d) A4.

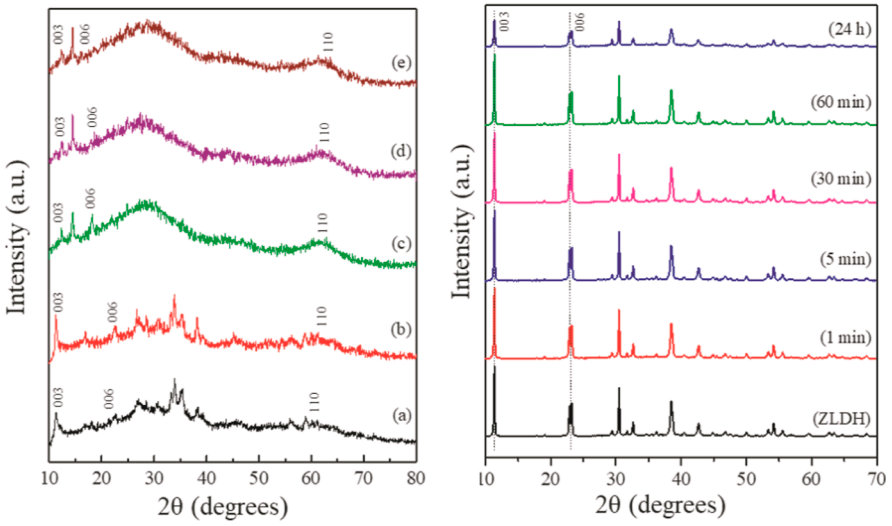

Figure 7. (Left) PXRD patterns for (a) ZAP1, (b) ZAP2, (c) ZAP3, (d) ZAP4, and (e) ZAP5; (right) PXRD of the ZLDH samples post sorption experiment for varied time with an initial IHP concentration of 0.0248 mM.

This critically indicates specific interaction occurring between the IHP moiety and the LDH component. The lowering of the peak intensity for Zn and Fe is observed because of the incurred change in the chemical environment around the metal ions due to the interaction with IHP. The shifting of the Zn 2p and Fe 2p peaks to higher binding energy values shows the adsorption of phytate at the surface through inner-sphere complex formation[56] (Figure 9), as already suggested by FTIR spectra. The increase in binding energy values signifies a lowering of electron density around the atoms.[57] Here, the LDH surface acted as Lewis acid and drew electron density from the negatively charged O atom of phytate group.[57] The deconvoluted XPS spectra of C1 s (sample ZAP5) exhibited characteristic peaks at 288.44, 286.13, and 284.69 eV binding energy values, interpreted as C═O, C−O, and C−C (H), respectively.[58,59] The XPS spectra of O 1s demonstrate a shift of 1.174 eV in the binding energy, essentially signifying the existence of adsorption.[60]

As is evident from the results, intercalation of the IHP moiety into the LDH interlayer spacing did not occur through anion exchange. Surface adsorption occurred between the highly charged anion and the positively charged LDH basal layers. This can be inferred to the complex size and very high charge density of IHP, for which the anionic moiety binds to the surface of the LDH without entering into the preformed LDH lamellar region.

The surface adsorption of IHP at the LDH surface is thus established from the facts mentioned above. The pattern and

https://doi.org/10.1021/acsomega.3c06788
ACS Omega 2023, 8, 43151−43162

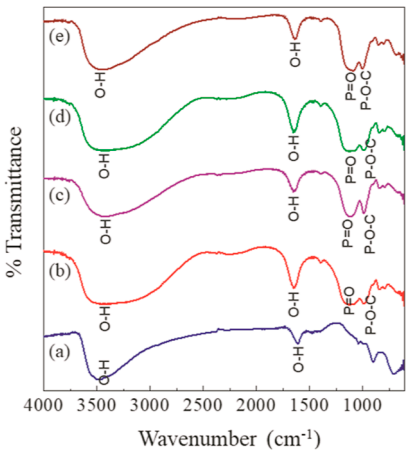

Figure 8. FTIR spectra for (a) ZAP1, (b) ZAP2, (c) ZAP3, (d) ZAP4, and (e) ZAP5.

mechanism of adsorption are further probed by conducting batch sorption experiments.

3.4. Sorption Isotherm and Kinetics. The sorption process was carried out with different initial IHP concentrations (~0.02−0.2 mM) at a temperature of 25 ± 0.5 °C. The adsorption capacity at equilibrium (Q_e) is observed to increase with time (Figure S8). In Figure 10a,b, the fitting of the sorption data is shown in linear form of Langmuir and Freundlich isotherm models, respectively. Table 4 represents the corresponding parameters from the isotherm and kinetic models and their correlation coefficients (R^2) with related standard errors (S.E.) for each parameter. Langmuir model fitted the experimental data best by linear analysis from the values of R^2 and related SE for each parameter (Table 4). The experimental data simulated with a pseudo-second-order kinetic model gave a good fit with R^2 = 0.99993 showcasing the adsorption process of IHP on Zn−Fe LDH to be in accordance with the pseudo-second-order rate eq (Figure 10c). The PXRD patterns (Figure 7) of the products obtained after sorption kinetic experiments exhibit a peak in good correspondence with the parent ZLDH, with peak positions and intensity remaining unchanged. This indicates no altercations in the LDH structures during the experiments. The diffraction patterns demonstrate evident difference from that obtained from anion exchange products. The lowering of intensity and peak broadening did not arise in the present case due to the use of lower IHP concentration and room temperature condition in kinetic experiments.

3.5. Zeta Potential (ζ) Measurement. The variation in zeta potential values of the ZLDH suspension before and after treatment with IHP as a function of pH is represented in Figure 11a. The zeta potential of the LDH suspension prior to treatment with IHP kept on decreasing with increasing pH. This occurs because of the OH^- groups present at the edges. Due to the protonation of the OH^- ions at lower pH, the edges become positively charged, and with positive basal surface, the whole particle represents a high positive ζ value.

At higher pH, deprotonation of the OH^- groups occurs, changing the sign on the edges to negative, resulting in flocculation occurring between the positively charged basal surface and negatively charged edges. Therefore, the ζ values lowered in higher pH values and eventually became negative at pH ~ 12, giving an isoelectric point (IEP) value at pH ~ 11. The low ζ value at pH 2 might result from dissolution of LDH in a highly acidic medium. The addition of highly negative IHP in all pH values led to inversion of the zeta potential and gave successively increasing—ζ values evidencing the adsorption of IHP occurring at the LDH surface due to electrostatic attraction arising between the highly negative IHP moiety and positively charged LDH basal surface.

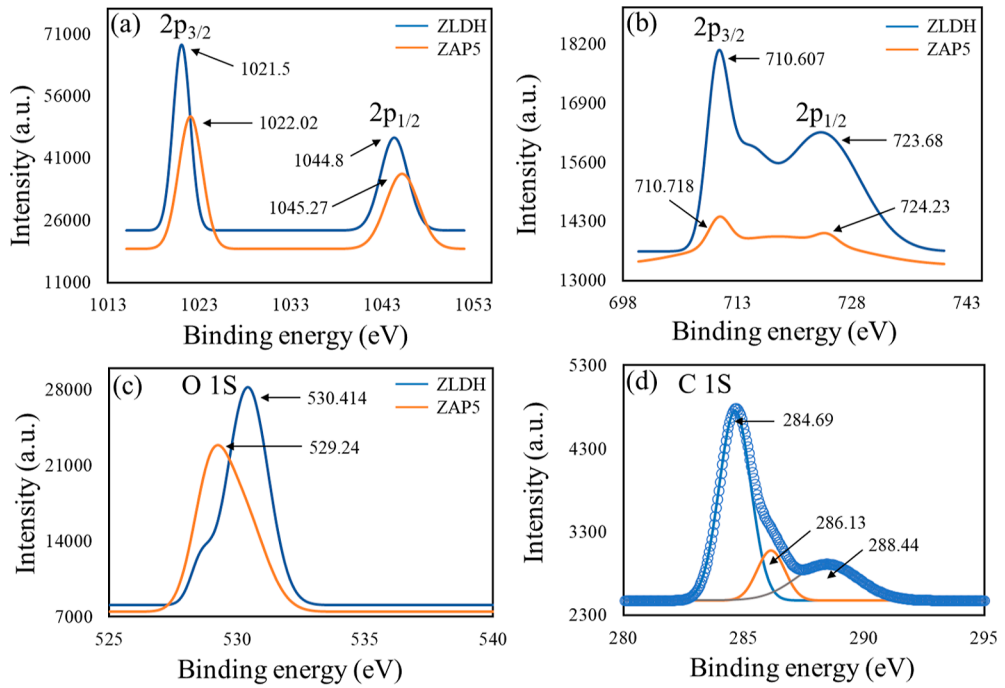

Figure 9. XPS spectra for shifting of (a) Zn 2p for ZLDH and ZAP5; (b) Fe 2p for ZLDH and ZAP5; (c) O 1s for ZLDH and ZAP5; and (d) C 1s deconvoluted spectra for ZAP5.

https://doi.org/10.1021/acsomega.3c06788
ACS Omega 2023, 8, 43151−43162

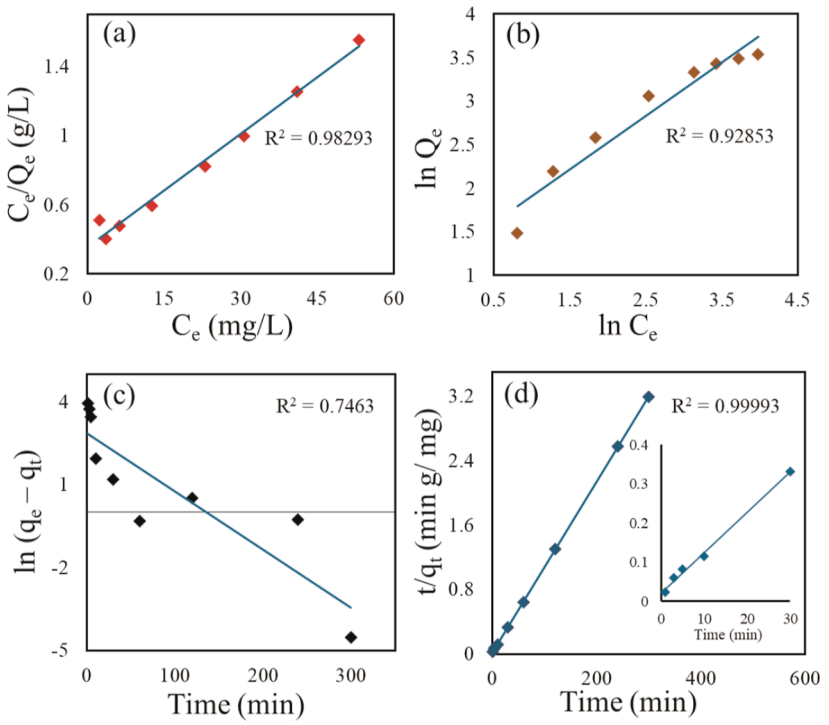

Figure 10. Sorption isotherm for IHP (a) Langmuir linear model (Langmuir linearization 1 plot of Hanes–Woolf plot), (b) Freundlich linear model, (c) pseudo-first-order sorption kinetic model, and (d) pseudo-second-order sorption kinetic model for IHP on ZLDH.

Table 4. Linear Isotherm and Kinetic Parameters for IHP Adsorption by ZLDH

model	parameters	units	value	S.E.
Langmuir linear model	Q_m	mg g^{-1}	45.87	0.00108
	K_L	L mg^{-1}	0.0613	003017
	R^2	_	0.98293	_
Freundlich linear model	K_F	_	3.6683	0.17983
	N	_	1.6312	0.06393
	R^2	_	0.92853	_
pseudo-first-order kinetic model	q_e	mg g^{-1}	17.558	0.5768
	k_1	min^{-1}	0.021	0.00424
	R^2	_	0.7463	_
Pseudo-second-order kinetic model	q_e	mg g^{-1}	94.25	3.2042×10^5
	k_2	g (mg min)$-^1$	0.00625	0.00436
	R^2	_	0.99993	_

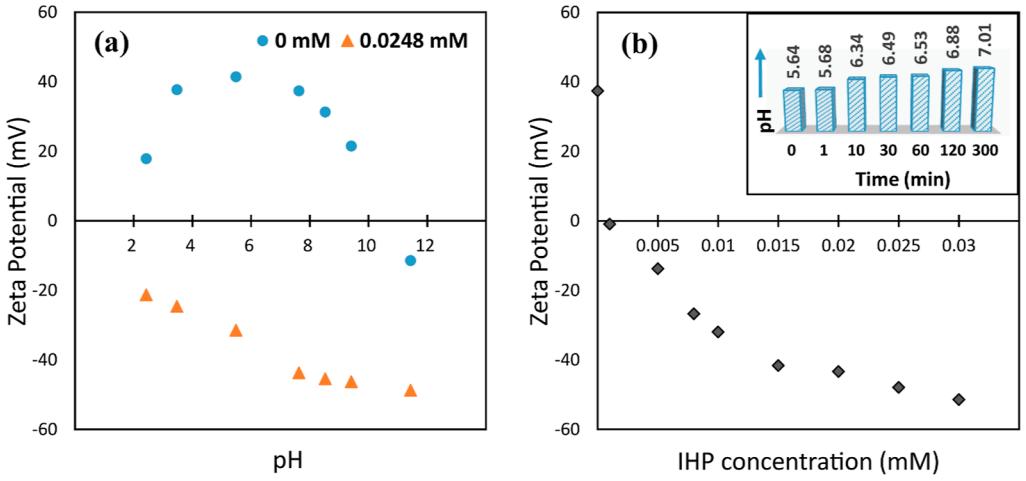

Figure 11. Zeta potential variation for (a) ZLDH suspension as a function of pH (with and without IHP) and (b) IHP concentration. [Inset: variation of pH of the LDH suspension after treatment with IHP solution with time].

https://doi.org/10.1021/acsomega.3c06788
ACS Omega 2023, 8, 43151−43162

Figure 11b shows the variation of ζ values with an increasing IHP concentration. A shift of the ζ value from +37.4 to −48.9 mV demonstrates (without outer interference of pH) that adsorption of IHP on LDH surface is a major contributing factor in altering the LDH surface to negative, and adsorption of IHP on LDH occurs through inner-sphere complex formation without the involvement of interlayer water molecules.[61,62] This fact is further supported by the pH values observed after sorption of IHP on the LDH suspension (recorded at definite time intervals, without tempering the initial pH of 5.63 of the system in the batch kinetic experiment).

From Figure 11 (inset), it is evident that the pH of the system shifted from 5.63 to 7.01 in 300 min. It can be deduced that the adsorption of IHP on the LDH surface occurs through ligand exchange route,[4] and the binding occurs through its PO_4^{3-} groups. During the interaction of the IHP moiety with the LDH metal centers, the OH^- ions and H_2O molecules are exchanged from the surface and released into the solution medium leading to the formation of inner-sphere complexes. This coincides well with the results obtained from the FTIR and XPS investigations. Moreover, the increased OH^- in solution as adsorption proceeds eventually increases the pH values in the medium, as observed from Figure 11 (inset).

$$M - OH + (IHP)^- \rightarrow M - (IHP) + OH^-$$

During the observation of the effect of IHP sorption with varying pH, the extent of sorption was found to decrease with increasing pH (Figure S9). This may be inferred to the fact that in higher pH, there would be fewer positive charges on the surface of ZLDH. Due to the deprotonation of basal OH^- of LDH, there would be greater OH^- in solution, which would compete with dissolved phytate under alkaline conditions. This corroborates the mechanism proposed by studying the zeta potential variations.

4. CONCLUSIONS

The investigation of intercalation of IHP in the Zn−Fe interlayers through coprecipitation and anion exchange method was performed with PXRD, FTIR, TGA, XPS, SEM−TEM, and ICP−MS analyses of the obtained products. Formation of IHP-intercalated Zn−Fe LDH with maximum d_{003} shift (1.375 nm) in PXRD spectra with a loading of 41.34% (w/w) was achieved through coprecipitation method in the pH range of ∼9−10. The expansion of the interlayer region was accompanied by a deformation of the conventional layered structure due to disordered stacking of the exfoliated nanosheets accommodating the rearranging IHP moiety in the basal spacing. The orientation of IHP in accordance with the stacking layers was evident to be in vertical alignment forming a monolayer between the basal surfaces by bonding through the PO_4^{3-} groups. Intercalation of IHP onto the layers of synthesized Zn−Fe LDH through anion exchange was not observed at all as suggested by the PXRD data. But the evidence from FTIR and XPS data, spectrophotometric assay, and measurement of variation of system pH and electrokinetic potential conveys rapid adsorption of IHP on the synthesized LDH surface through monolayer formation. The existence of electrostatic attraction and inner-sphere complex formation through ligand exchange mechanism were observed to be responsible for the sorption of IHP on ZLDH surface. The batch sorption experimental data followed pseudo-second-order kinetic model and gave a good fit with the Langmuir isotherm with a maximum adsorption capacity of 45.87 mg g^{-1}.

■ ASSOCIATED CONTENT

Supporting Information

The Supporting Information is available free of charge at https://pubs.acs.org/doi/10.1021/acsomega.3c06788.

Cartesian coordinates for optimized phytic acid structure, bond distances calculated from the optimized structure, EDX spectra (ZLDH and Z1), elemental composition of ZLDH and Z1 from EDX analysis, XPS spectra (ZLDH, Z1, ZAP1, and ZAP5), XPS spectra for Zn and Fe in ZLDH, deconvoluted XPS spectra (C 1s for ZLDH and Z1; O 1s for ZLDH, Z1, and ZAP5), HRTEM images for ZLDH and Z1, FTIR spectra (Z2-Z5), variation of adsorption capacity with pH and time, and PXRD pattern for reconstruction of ZLDH in sodium phytate solution (PDF)

■ AUTHOR INFORMATION

Corresponding Authors

Jiban Saikia − *Department of Chemistry, Dibrugarh University, Dibrugarh 786004 Assam, India;* orcid.org/0000-0002-7422-9006; Phone: 9706379107; Email: jibansaikia@dibru.ac.in

Tanmoy Karak − *Department of Soil Science, School of Agricultural Sciences, Nagaland University, Medziphema Campus 797106 Nagaland, India*; Email: tanmoy@nagalanduniversity.ac.in

Authors

Rimjim Gogoi − *Department of Chemistry, Dibrugarh University, Dibrugarh 786004 Assam, India*

Madhusmita Baruah − *Department of Chemistry, Dibrugarh University, Dibrugarh 786004 Assam, India*

Arup Borgohain − *Department of Chemistry, Dibrugarh University, Dibrugarh 786004 Assam, India*

Vishwa Jyoti Baruah − *Centre for Biotechnology and Bioinformatics, Dibrugarh University, Dibrugarh 786004 Assam, India;* orcid.org/0000-0003-0583-6205

Satter Rohman − *Department of Chemistry, Dibrugarh University, Dibrugarh 786004 Assam, India;* orcid.org/0000-0001-7573-9262

Mohini Singh − *Department of Pharmaceutical Sciences, Dibrugarh University, Dibrugarh 786004 Assam, India*

Rahul Kar − *Department of Chemistry, Dibrugarh University, Dibrugarh 786004 Assam, India*

Sandeep Kumar Dey − *CSIR-North East Institute of Science and Technology, Jorhat 785006 Assam, India*

Bhaskar Mazumder − *Department of Pharmaceutical Sciences, Dibrugarh University, Dibrugarh 786004 Assam, India*

Complete contact information is available at: https://pubs.acs.org/10.1021/acsomega.3c06788

Author Contributions

The manuscript was written through the contributions of all authors. All authors have given approval to the final version of the manuscript.

Notes

The authors declare no competing financial interest.

https://doi.org/10.1021/acsomega.3c06788
ACS Omega 2023, 8, 43151−43162

■ ACKNOWLEDGMENTS

The authors are immensely grateful toward the Department of Biotechnology, India for providing financial assistance (under project no. BT/PR36255/NNT/28/1728/2020). The authors also acknowledge the Department of Science and Technology for financial aid under DST-FIST programme and DST-PURSE programme [no. SR/PURSE/2022/143 (C)], and UGC, New Delhi for Special Assistance Program (UGC-SAP) to the Department of Chemistry, Dibrugarh University. Authors acknowledge the CSIC Dibrugarh University and STIC Kochi for analytical support.

■ REFERENCES

(1) Weeks, J. J.; Hettiarachchi, G. M. A Review of the Latest in Phosphorus Fertilizer Technology: Possibilities and Pragmatism. *J. Environ. Qual.* **2019**, *48* (5), 1300−1313.

(2) Guan, X. H.; Shang, C.; Zhu, J.; Chen, G. H. ATR-FTIR Investigation on the Complexation of Myo-Inositol Hexaphosphate with Aluminum Hydroxide. *J. Colloid Interface Sci.* **2006**, *293* (2), 296−302.

(3) Zhu, Y.; Liu, Z.; Luo, K.; Xie, F.; He, Z.; Liao, H.; Giesy, J. P. The Adsorption of Phytate onto an Fe-Al-La Trimetal Composite Adsorbent: Kinetics, Isotherms, Mechanism and Implication. *Environ. Sci.: Water Res. Technol.* **2021**, *7* (11), 1971−1984.

(4) Wang, W.; Tan, J.; Li, S.; Guan, Y.; Zhang, X.; Wang, N.; Liu, J.; Jiang, X. Transport, Retention and Release of Phytate in Soil with Addition of Mg-Al Layered Double Hydroxides. *J. Cleaner Prod.* **2022**, *379*, 134774.

(5) Ognalaga, M.; Frossard, E.; Thomas, F. Glucose-1-Phosphate and Myo-Inositol Hexaphosphate Adsorption Mechanisms on Goethite. *Soil Sci. Soc. Am. J.* **1994**, *58* (2), 332−337.

(6) Celi, L.; Presta, M.; Ajmore-Marsan, F.; Barberis, E. Effects of PH and Electrolytes on Inositol Hexaphosphate Interaction with Goethite. *Soil Sci. Soc. Am. J.* **2001**, *65* (3), 753−760.

(7) Kremer, C.; Torres, J.; Bianchi, A.; Savastano, M.; Bazzicalupi, C. Myo-Inositol Hexakisphosphate: Coordinative Versatility of a Natural Product. *Coord. Chem. Rev.* **2020**, *419*, 213403.

(8) Yan, Y.; Li, W.; Yang, J.; Zheng, A.; Liu, F.; Feng, X.; Sparks, D. L. Mechanism of Myo-Inositol Hexakisphosphate Sorption on Amorphous Aluminum Hydroxide: Spectroscopic Evidence for Rapid Surface Precipitation. *Environ. Sci. Technol.* **2014**, *48* (12), 6735−6742.

(9) Wang, L.; Putnis, C. V.; King, H. E.; Hövelmann, J.; Ruiz-Agudo, E.; Putnis, A. Imaging Organophosphate and Pyrophosphate Sequestration on Brucite by in Situ Atomic Force Microscopy. *Environ. Sci. Technol.* **2017**, *51* (1), 328−336.

(10) Yan, Y.; Koopal, L. K.; Li, W.; Zheng, A.; Yang, J.; Liu, F.; Feng, X. Size-Dependent Sorption of Myo-Inositol Hexakisphosphate and Orthophosphate on Nano-γ-Al2O3. *J. Colloid Interface Sci.* **2015**, *451*, 85−92.

(11) Yan, Y.; Koopal, L. K.; Liu, F.; Huang, Q.; Feng, X. Desorption of Myo-Inositol Hexakisphosphate and Phosphate from Goethite by Different Reagents. *J. Plant Nutr. Soil Sci.* **2015**, *178* (6), 878−887.

(12) Yan, Y.; Wan, B.; Liu, F.; Tan, W.; Liu, M.; Feng, X. Adsorption-Desorption of Myo-Inositol Hexakisphosphate on Hematite. *Soil Sci.* **2014**, *179* (10−11), 476−485.

(13) Celi, L.; De Luca, G.; Barberis, E. Effects of interaction of organic and inorganic P with Ferrihydrite and Kaolinite-iron oxide systems on iron release. *Soil Sci.* **2003**, *168* (7), 479−488.

(14) Hu, Z.; Jaisi, D. P.; Yan, Y.; Chen, H.; Wang, X.; Wan, B.; Liu, F.; Tan, W.; Huang, Q.; Feng, X. Adsorption and Precipitation of Myo-Inositol Hexakisphosphate onto Kaolinite. *Eurasian J. Soil Sci.* **2020**, *71* (2), 226−235.

(15) Bugris, V.; Haspel, H.; Kukovecz, Á.; Kónya, Z.; Sipiczki, M.; Sipos, P.; Pálinkó, I. Water Types and Their Relaxation Behavior in Partially Rehydrated CaFe-Mixed Binary Oxide Obtained from CaFe-Layered Double Hydroxide in the 155−298 K Temperature Range. *Langmuir* **2013**, *29* (43), 13315−13321.

(16) Halajnia, A.; Oustan, S.; Najafi, N.; Khataee, A. R.; Lakzian, A. The Adsorption Characteristics of Nitrate on Mg-Fe and Mg-Al Layered Double Hydroxides in a Simulated Soil Solution. *Appl. Clay Sci.* **2012**, *70*, 28−36.

(17) Zhao, H.; Nagy, K. L. Dodecyl Sulfate-Hydrotalcite Nanocomposites for Trapping Chlorinated Organic Pollutants in Water. *J. Colloid Interface Sci.* **2004**, *274* (2), 613−624.

(18) Jadam, M. L.; Syed Mohamad, S. A.; Zaki, H. M.; Jubri, Z.; Sarijo, S. H. Antibacterial Activity and Physicochemical Characterization of Calcium-Aluminium-Ciprofloxacin-Layered Double Hydroxide. *J. Drug Delivery Sci. Technol.* **2021**, *62*, 102314.

(19) Lundehøj, L.; Cellier, J.; Forano, C.; Nielsen, U. G. Atomic Level Understanding of Orthophosphate Adsorption by Magnesium Aluminum-Layered Double Hydroxides - A Multitechnique Study. *J. Phys. Chem. C* **2019**, *123* (39), 24039−24050.

(20) Benício, L. P. F.; Constantino, V. R. L.; Pinto, F. G.; Vergütz, L.; Tronto, J.; Da Costa, L. M. Layered Double Hydroxides: New Technology in Phosphate Fertilizers Based on Nanostructured Materials. *ACS Sustain. Chem. Eng.* **2017**, *5* (1), 399−409.

(21) Bernardo, M. P.; Guimarães, G. G. F.; Majaron, V. F.; Ribeiro, C. Controlled Release of Phosphate from Layered Double Hydroxide Structures: Dynamics in Soil and Application as Smart Fertilizer. *ACS Sustain. Chem. Eng.* **2018**, *6* (4), 5152−5161.

(22) Berber, M. R.; Hafez, I. H. Synthesis of a New Nitrate-Fertilizer Form with a Controlled Release Behavior via an Incorporation Technique into a Clay Material. *Bull. Environ. Contam. Toxicol.* **2018**, *101* (6), 751−757.

(23) Songkhum, P.; Wuttikhun, T.; Chanlek, N.; Khemthong, P.; Laohhasurayotin, K. Controlled Release Studies of Boron and Zinc from Layered Double Hydroxides as the Micronutrient Hosts for Agricultural Application. *Appl. Clay Sci.* **2018**, *152*, 311−322.

(24) Woo, M. A.; Woo Kim, T.; Paek, M. J.; Ha, H. W.; Choy, J. H.; Hwang, S. J. Phosphate-Intercalated CaFe-Layered Double Hydroxides: Crystal Structure, Bonding Character, and Release Kinetics of Phosphate. *J. Solid State Chem.* **2011**, *184* (1), 171−176.

(25) de Sousa, A. L. M. D.; dos Santos, W. M.; de Souza, M. L.; Silva, L. C. P. B. B.; Yun, A. E. H. K.; Aguilera, C. S. B.; Chagas, B. d. F.; Rolim, L. A.; da Silva, R. M. F.; Neto, P. J. R. Layered Double Hydroxides as Promising Excipients for Drug Delivery Purposes. *Eur. J. Pharm. Sci.* **2021**, *165*, 105922.

(26) Usman, M. S.; Hussein, M. Z.; Fakurazi, S.; Ahmad Saad, F. F. Gadolinium-Based Layered Double Hydroxide and Graphene Oxide Nano-Carriers for Magnetic Resonance Imaging and Drug Delivery. *Chem. Cent. J.* **2017**, *11*, 47.

(27) Senapati, S.; Thakur, R.; Verma, S. P.; Duggal, S.; Mishra, D. P.; Das, P.; Shripathi, T.; Kumar, M.; Rana, D.; Maiti, P. Layered Double Hydroxides as Effective Carrier for Anticancer Drugs and Tailoring of Release Rate through Interlayer Anions. *J. Controlled Release* **2016**, *224*, 186−198.

(28) Jin, C.; Liu, H.; Kong, X.; Yan, H.; Lei, X. Enrichment of Rare Earth Metal Ions by the Highly Selective Adsorption of Phytate Intercalated Layered Double Hydroxide. *Dalton Trans.* **2018**, *47* (9), 3093−3101.

(29) Mohammadi, A.; Hosseini, D.; Isfahani, A. P.; Dehghani, Z.; Shams, E. Waterborne Polyurethane Nanocomposite Incorporated with Phytic Acid Intercalated Layered Double Hydroxides: A Highly Stable Aqueous Dispersion with Desired Corrosion Protection Capability. *Polym. Adv. Technol.* **2021**, *32* (10), 4014−4028.

(30) Jin, X.; Gu, X.; Chen, C.; Tang, W.; Li, H.; Liu, X.; Bourbigot, S.; Zhang, Z.; Sun, J.; Zhang, S. The Fire Performance of Polylactic Acid Containing a Novel Intumescent Flame Retardant and Intercalated Layered Double Hydroxides. *J. Mater. Sci.* **2017**, *52* (20), 12235−12250.

(31) Zhang, H.; Wen, X.; Wang, Y. Synthesis and Characterization of Sulfate and Dodecylbenzenesulfonate Intercalated Zinc-Iron Layered Double Hydroxides by One-Step Coprecipitation Route. *J. Solid State Chem.* **2007**, *180* (5), 1636−1647.

https://doi.org/10.1021/acsomega.3c06788
ACS Omega 2023, 8, 43151−43162

(32) Wang, Q.; Lin, Q.; Li, Q.; Li, K.; Wu, L.; Li, S.; Liu, H. As(III) Removal from Wastewater and Direct Stabilization by in-Situ Formation of Zn-Fe Layered Double Hydroxides. *J. Hazard. Mater.* **2021**, *403*, 123920.
(33) Li, C.; Wan, J.; Kalali, E. N.; Fan, H.; Wang, D. Y. Synthesis and Characterization of Functional Eugenol Derivative Based Layered Double Hydroxide and Its Use as a Nanoflame-Retardant in Epoxy Resin. *J. Mater. Chem. A* **2015**, *3* (7), 3471−3479.
(34) Anbarasan, R.; Lee, W. D.; Im, S. S. Adsorption and Intercalation of Anionic Surfactants onto Layered Double Hydroxides-XRD Study. *Bull. Mater. Sci.* **2005**, *28* (2), 145−149.
(35) Agostinho, A. J.; de Souza Oliveira, W.; Anunciação, D. S.; Santos, J. C. C. Simple and Sensitive Spectrophotometric Method for Phytic Acid Determination in Grains. *Food Anal. Methods* **2016**, *9* (7), 2087−2096.
(36) Chakraborty, A.; Acharya, H. Selective Removal of Anionic Dyes by Metal-Organic Framework-Anchored CoAl-Layered Double Hydroxide Nanosheets. *ACS Appl. Nano Mater.* **2021**, *4* (11), 12561−12575.
(37) Darmograi, G.; Prelot, B.; Layrac, G.; Tichit, D.; Martin-Gassin, G.; Salles, F.; Zajac, J. Study of Adsorption and Intercalation of Orange-Type Dyes into Mg-Al Layered Double Hydroxide. *J. Phys. Chem. C* **2015**, *119* (41), 23388−23397.
(38) Wang, X.; Hu, Y.; Tang, Y.; Yang, P.; Feng, X.; Xu, W.; Zhu, M. Phosphate and Phytate Adsorption and Precipitation on Ferrihydrite Surfaces. *Environ. Sci.: Nano* **2017**, *4* (11), 2193−2204.
(39) Chen, X. Modeling of Experimental Adsorption Isotherm Data. *Information* **2015**, *6* (1), 14−22.
(40) Frisch, M. J.; Trucks, G. W.; Schlegel, H. B.; Scuseria, G. E.; Robb, M. A.; Cheeseman, J. R.; Scalmani, G.; Barone, V.; Mennucci, B.; Petersson, G. A.; Nakatsuji, H.; Caricato, M.; Li, X.; Hratchian, H. P.; Izmaylov, A. F.; Bloino, J.; Zheng, G.; Sonnenberg, J. L.; Hada, M.; Ehara, M.; Toyota, K.; Fukuda, R.; Hasegawa, J.; Ishida, M.; Nakajima, T.; Honda, Y.; Kitao, O.; Nakai, H.; Vreven, T.; Montgomery, Jr., J. A.; Peralta, J. E.; Ogliaro, F.; Bearpark, M.; Heyd, J.; Brothers, E.; Kudin, K. N.; Staroverov, V. N.; Kobayashi, R.; Normand, J.; Raghavachari, K.; Rendell, A.; Burant, J. C.; Iyengar, S. S.; Tomasi, J.; Cossi, M.; Rega, N.; Millam, J. M.; Klene, M.; Knox, J. E.; Cross, J. B.; Bakken, V.; Adamo, C.; Jaramillo, J.; Gomperts, R.; Stratmann, R. E.; Yazyev, O.; Austin, A. J.; Cammi, R.; Pomelli, C.; Ochterski, J. W.; Martin, R. L.; Morokuma, K.; Zakrzewski, V. G.; Voth, G. A.; Salvador, P.; Dannenberg, J. J.; Dapprich, S.; Daniels, A. D.; Farkas, O.; Foresman, J. B.; Ortiz, J. V.; Cioslowski, J.; Fox, D. J. *Gaussian 09*; Gaussian, Inc.: Wallingford, CT, 2009.
(41) Chakraborty, M.; Dasgupta, S.; Soundrapandian, C.; Chakraborty, J.; Ghosh, S.; Mitra, M. K.; Basu, D. Methotrexate Intercalated ZnAl-Layered Double Hydroxide. *J. Solid State Chem.* **2011**, *184* (9), 2439−2445.
(42) Alibakhshi, E.; Ghasemi, E.; Mahdavian, M.; Ramezanzadeh, B.; Farashi, S. Fabrication and Characterization of PO_4^{3-} Intercalated Zn-Al- Layered Double Hydroxide Nanocontainer. *J. Electrochem. Soc.* **2016**, *163* (8), 495−505.
(43) Al-Jaberi, M.; Naille, S.; Dossot, M.; Ruby, C. Interlayer Interaction in Ca-Fe Layered Double Hydroxides Intercalated with Nitrate and Chloride Species. *J. Mol. Struct.* **2015**, *1102*, 253−260.
(44) Fahami, A.; Al-Hazmi, F. S.; Al-Ghamdi, A. A.; Mahmoud, W. E.; Beall, G. W. Structural Characterization of Chlorine Intercalated Mg-Al Layered Double Hydroxides: A Comparative Study between Mechanochemistry and Hydrothermal Methods. *J. Alloys Compd.* **2016**, *683*, 100−107.
(45) Gupta, N. K.; Saifuddin, M.; Kim, S.; Kim, K. S. Microscopic, Spectroscopic, and Experimental Approach towards Understanding the Phosphate Adsorption onto Zn-Fe Layered Double Hydroxide. *J. Mol. Liq.* **2020**, *297*, 111935.
(46) Fleutot, S.; Dupin, J. C.; Renaudin, G.; Martinez, H. Intercalation and Grafting of Benzene Derivatives into Zinc-Aluminum and Copper-Chromium Layered Double Hydroxide Hosts: An XPS Monitoring Study. *Phys. Chem. Chem. Phys.* **2011**, *13* (39), 17564−17578.
(47) Zhou, H.; Jiang, Z.; Wei, S.; Liang, J. Adsorption of Cd(II) from Aqueous Solutions by a Novel Layered Double Hydroxide FeMnMg-LDH. *Water, Air, Soil Pollut.* **2018**, *229* (3), 78.
(48) Dao, T. L. K.; Tieu, A. K.; Tran, B. H.; Pham, S. T. Influence of Structural Disorders on the Tribological Behavior of Phosphate-Intercalated Layered Double Hydroxide Additives in Polyalphaolefin. *Langmuir* **2022**, *38* (27), 8416−8427.
(49) Ay, A. N.; Zümreoglu-Karan, B.; Temel, A.; Mafra, L. Layered Double Hydroxides with Interlayer Borate Anions: A Critical Evaluation of Synthesis Methodology and PH-Independent Orientations in Nano-Galleries. *Appl. Clay Sci.* **2011**, *51* (3), 308−316.
(50) Dupin, J. C.; Martinez, H.; Guimon, C.; Dumitriu, E.; Fechete, I. Intercalation Compounds of Mg-Al Layered Double Hydroxides with Dichlophenac: Different Methods of Preparation and Physico-Chemical Characterization. *Appl. Clay Sci.* **2004**, *27* (1−2), 95−106.
(51) Cavani, F.; Trifirb, F.; Vaccari, A. Hydrotalcite-type anlonlc clays: Preparation, properties and applications. *Catal. Today* **1991**, *11* (2), 173−301.
(52) Bukhtiyarova, M. V. A Review on Effect of Synthesis Conditions on the Formation of Layered Double Hydroxides. *J. Solid State Chem.* **2019**, *269*, 494−506.
(53) Theiss, F. L.; Ayoko, G. A.; Frost, R. L. Synthesis of Layered Double Hydroxides Containing Mg^{2+}, Zn^{2+}, Ca^{2+} and Al^{3+} Layer Cations by Co-Precipitation Methods - A Review. *Appl. Surf. Sci.* **2016**, *383*, 200−213.
(54) Rami, J. M.; Patel, C. D.; Patel, C. M.; Patel, M. V. Thermogravimetric Analysis (TGA) of Some Synthesized Metal Oxide Nanoparticles. *Mater. Today: Proc.* **2021**, *43*, 655−659.
(55) Aisawa, S.; Takahashi, S.; Ogasawara, W.; Umetsu, Y.; Narita, E. Direct Intercalation of Amino Acids into Layered Double Hydroxides by Coprecipitation. *J. Solid State Chem.* **2001**, *162* (1), 52−62.
(56) Li, A.; Deng, H.; Ye, C.; Jiang, Y. Fabrication and Characterization of Novel ZnAl-Layered Double Hydroxide for the Superadsorption of Organic Contaminants from Wastewater. *ACS Omega* **2020**, *5* (25), 15152−15161.
(57) Wei, J.; Zhang, W.; Pan, W.; Li, C.; Sun, W. Experimental and Theoretical Investigations on Se(IV) and Se(VI) Adsorption to UiO-66-Based Metal-Organic Frameworks. *Environ. Sci.: Nano* **2018**, *5* (6), 1441−1453.
(58) Li, S. S.; Jiang, M.; Jiang, T. J.; Liu, J. H.; Guo, Z.; Huang, X. J. Competitive Adsorption Behavior toward Metal Ions on Nano-Fe/Mg/Ni Ternary Layered Double Hydroxide Proved by XPS: Evidence of Selective and Sensitive Detection of Pb(II). *J. Hazard. Mater.* **2017**, *338*, 1−10.
(59) Younes, H. A.; Khaled, R.; Mahmoud, H. M.; Nassar, H. F.; Abdelrahman, M. M.; Abo El-Ela, F. I.; Taha, M. Computational and Experimental Studies on the Efficient Removal of Diclofenac from Water Using ZnFe-Layered Double Hydroxide as an Environmentally Benign Absorbent. *J. Taiwan Inst. Chem. Eng.* **2019**, *102*, 297−311.
(60) Liang, X.; Hou, W.; Xu, Y.; Sun, G.; Wang, L.; Sun, Y.; Qin, X. Sorption of Lead Ion by Layered Double Hydroxide Intercalated with Diethylenetriaminepentaacetic Acid. *Colloids Surf., A* **2010**, *366* (1−3), 50−57.
(61) Xu, Z. P.; Jin, Y.; Liu, S.; Hao, Z. P.; Lu, G. Q. M. Surface Charging of Layered Double Hydroxides during Dynamic Interactions of Anions at the Interfaces. *J. Colloid Interface Sci.* **2008**, *326* (2), 522−529.
(62) Zhang, Y.; Evans, J. R. G. Alignment of Layered Double Hydroxide Platelets. *Colloids Surf., A* **2012**, *408*, 71−78.

https://doi.org/10.1021/acsomega.3c06788
ACS Omega 2023, 8, 43151−43162